

Deep learning-enabled inverse design of polarization-selective structural color based on coding metasurface

Haolin Yang(杨昊霖), Bo Ni(倪波), Junhong Guo(郭俊宏), Hua Zhou(周华), and Jianhua Chang(常建华)

Citation: Chin. Phys. B, 2025, 34 (**5**): 050702. DOI: 10.1088/1674-1056/adb94a
Journal homepage: http://cpb.iphy.ac.cn; http://iopscience.iop.org/cpb

What follows is a list of articles you may be interested in

Causally enhanced initial conditions: A novel soft constraints strategy for physics informed neural networks

Wenshu Zha(查文舒), Dongsheng Chen(陈东升), Daolun Li(李道伦), Luhang Shen(沈路航), and Enyuan Chen(陈恩源)
Chin. Phys. B, 2025, 34 (**4**): 040701. DOI: 10.1088/1674-1056/adacd0

Image segmentation of exfoliated two-dimensional materials by generative adversarial network-based data augmentation

Xiaoyu Cheng(程晓昱), Chenxue Xie(解晨雪), Yulun Liu(刘宇伦), Ruixue Bai(白瑞雪), Nanhai Xiao(肖南海), Yanbo Ren(任琰博), Xilin Zhang(张喜林), Hui Ma(马惠), and Chongyun Jiang(蒋崇云)
Chin. Phys. B, 2024, 33 (**3**): 030703. DOI: 10.1088/1674-1056/ad23d8

Recent advances in protein conformation sampling by combining machine learning with molecular simulation

Yiming Tang(唐一鸣), Zhongyuan Yang(杨中元), Yifei Yao(姚逸飞), Yun Zhou(周运), Yuan Tan(谈圆),Zichao Wang(王子超), Tong Pan(潘瞳), Rui Xiong(熊瑞), Junli Sun(孙俊力), and Guanghong Wei(韦广红)
Chin. Phys. B, 2024, 33 (**3**): 030701. DOI: 10.1088/1674-1056/ad1a92

Crysformer: An attention-based graph neural network for properties prediction of crystals

Tian Wang(王田), Jiahui Chen(陈家辉), Jing Teng(滕婧), Jingang Shi(史金钢),Xinhua Zeng(曾新华), and Hichem Snoussi
Chin. Phys. B, 2023, 32 (**9**): 090703. DOI: 10.1088/1674-1056/ace247

Differentiable programming and density matrix based Hartree-Fock method

Hong-Bin Ren(任宏斌), Lei Wang(王磊), and Xi Dai(戴希)
Chin. Phys. B, 2021, 30 (**6**): 060701. DOI: 10.1088/1674-1056/abeeed

---

Deep learning-enabled inverse design of polarization-selective structural color based on coding metasurface

Haolin Yang(杨昊霖)[1], Bo Ni(倪波)[1], Junhong Guo(郭俊宏)[2], Hua Zhou(周华)[1,†], and Jianhua Chang(常建华)[1]

[1] *Jiangsu Key Laboratory of Meteorological Observation and Information Processing, School of Electronic and Information Engineering, Nanjing University of Information Science and Technology, Nanjing* 210044, *China*

[2] *College of Electronic and Optical Engineering and College of Flexible Electronics (Future Technology), Nanjing University of Posts and Telecommunications, Nanjing* 210023, *China*

(Received 6 December 2024; revised manuscript received 5 February 2025; accepted manuscript online 24 February 2025)

Structural colors based on metasurfaces have very promising applications in areas such as optical image encryption and color printing. Herein, we propose a deep learning-enabled reverse design of polarization-selective structural color based on coding metasurface. In this study, the long short-term memory (LSTM) neural network is presented to enable the forward and inverse mapping between coding metasurface structure and corresponding color. The results show that the method can achieve 98% accuracy for the forward prediction of color and 93% accuracy for the inverse design of the structure. Moreover, a cascaded architecture is adopted to train the inverse neural network model, which can solve the non-uniqueness problem of the polarization-selective color reverse design. This study provides a new path for the application and development of structural colors.

Keywords: deep learning, inverse design, coding metasurface, structural color, polarization-selective

PACS: 07.05.Mh, 78.20.Bh, 78.67.Pt, 42.79.–e

DOI: 10.1088/1674-1056/adb94a **CSTR:** 32038.14.CPB.adb94a

1. Introduction

Metasurfaces are artificial structures made of periodic or non-periodic arrangements of sub-wavelength-sized cells, which possess very excellent optical field modulation properties.[1,2] The structural units of conventional metasurface are usually cylinders,[3,4] bores,[5,6] nanorods,[7,8] split rings,[9,10] etc. In 2014, Tiejun Cui's team first proposed the novel concept of "coding metasurface",[11] which requires fewer cells to be designed than conventional metasurface but is more flexible in electromagnetic wave modulation. In recent years, metasurface has been widely used in the field of structural color design.[12–15] Structural colors based on metasurface can be divided into two parts, polarization-independent structural colors and polarization-selective structural colors. Polarization-independent metasurface structural colors are mainly used in the field of high-precision image display,[16,17] and polarization-selective metasurface structural colors are mainly used in the field of realizing optical encryption of images or anti-counterfeiting.[18,19]

Mostly, the metasurface structural colors are designed by the full electromagnetic simulation, such as finite element method (FEM)[20,21] or finite difference time domain method (FDTD).[22,23] The metasurface structural color that presents a particular target color can be obtained by changing the geometry or structural size of its micro and nano elements.[17,24] This inevitably leads to a huge amount of time and computational power required for the design of complex nanostructures. Therefore, the design of metasurface structural colors based on such methods is limited in practical applications.

In recent years, the application of deep learning in micro–nano photonics has attracted much attention. Deep learning methods can realize forward prediction of optical response[25–27] or inverse design of micro–nano structures[28–30] in a very short time. Particularly, in 2019, recurrent neural networks (RNN), which is one of the branches of deep learning, was used to realize the inverse design of structural color by accomplishing the prediction of absorption spectra generated by random silver micro–nano structures.[31] However, it can only cover a small range of color regions. In 2022, as a superior form of RNN, long short term memory (LSTM) neural network was used to achieve the inverse design of structural color based on Si metasurface structure.[32] The structure can achieve large coverage of colors, but it requires changing the structural size of the entire metasurface device. In 2024, Ma Taigao *et al.* proposed a reverse design method for multilayer thin-film-based structures called OptoGPT, which can achieve an extremely rich optical functionality by taking the target spectra as the input and the serialized physical structure and thickness of the materials as the output. However, the variety of materials required and the uncer-

†Corresponding author. E-mail: hzhou@nuist.edu.cn

© 2025 Chinese Physical Society and IOP Publishing Ltd. All rights, including for text and data mining, AI training, and similar technologies, are reserved.

tainty in the thickness of each material will lead to a considerable engineering cost in the actual production application of the structure's color at considerable engineering cost in practical production applications.[33] Therefore, fast design of structural colors based on deep learning to achieve a large range of color coverage is still a worthy research problem.

In this paper, a polarization-selective coding metasurface structural color inverse design by combining deep learning and coding metasurface based on LSTM networks is proposed and investigated. The metasurface structural colors designed can cover mostly regions of the standard color space (sRGB) in the CIE 1931 chromaticity diagram without increasing the size and complexity of the device structure. In addition, by referring to feedback mechanisms in supervised learning, a cascaded architecture is adopted to train the inverse neural network model, which can solve the non-uniqueness problem in reverse design. This inverse design method can design the encoding parameters of the polarization-selective coding metasurface corresponding to tens of thousands of target colors in 10 s with 93% accuracy. Lastly, the optical encryption of color images with certain text information is realized, based on the reverse design model.

2. Structure and design

2.1. Structure and dataset

Figure 1(a) shows a schematic structure of the coding metasurface. The schematic contains four identical 10×10 coding units, demonstrating the polarization-selective properties of the same coding unit that will produce different colors of reflected light at different polarization angles of incidence of white light. The bottom layer of each coding unit is Ag, the middle layer is SiO_2 and the top layer is the coding metasurface structure. The single 0/1 coding structure consists of Ag–Si_3N_4 composite columns. The presence of a composite structure indicates a "1", while the vacancy indicates a "0". The length and width of the Ag–Si_3N_4 composite column are $l_x = 30$ nm and $l_y = 30$ nm, and the height $h_1 = 200$ nm and $h_2 = 40$ nm; the thickness of the SiO_2 and Ag layers are $h_3 = 50$ nm and $h_4 = 120$ nm, respectively, and the period of the coding structure is $p = 300$ nm. The refractive index data of the materials used are obtained from Palik.[34]

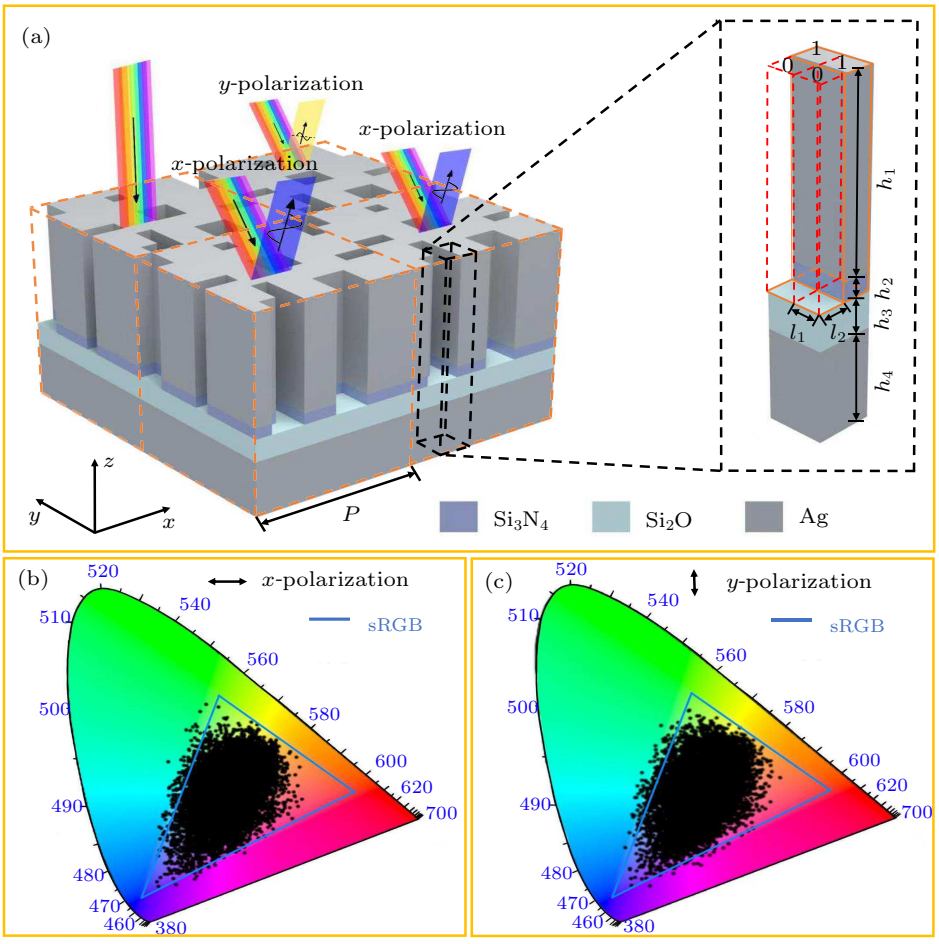


Fig. 1. (a) Schematic diagram of the polarization-selective coding metasurface and the structure of the coding cell. (b)–(c) The coverage of the 12000 coding structures of this polarization-selective coding metasurface in the two orthogonal polarization directions for the colors presented on the CIE 1931 chromaticity diagram, (b) x polarization direction, and (c) y polarization direction.

The coding metasurface on the top is generated by random 0/1 code. The 13200 groups' reflectance spectra in x and y polarization directions with different coding forms are obtained by using the FDTD simulation. Among them, 12000 sets of data are used as the learning datasets of the training network, and the remaining 1200 sets of data are used as the test data.

Based on the spectral information, the tristimulus values are calculated according to the following equations:[35]

$$X = \frac{\int_\lambda I_{\mathrm{D65}}(\lambda)\, T(\lambda)\, \bar{x}(\lambda)\, \mathrm{d}\lambda}{\int_\lambda I_{\mathrm{D65}}(\lambda)\, \bar{y}(\lambda)\, \mathrm{d}\lambda}, \tag{1}$$

$$Y = \frac{\int_\lambda I_{\mathrm{D65}}(\lambda)\, T(\lambda)\, \bar{y}(\lambda)\, \mathrm{d}\lambda}{\int_\lambda I_{\mathrm{D65}}(\lambda)\, \bar{y}(\lambda)\, \mathrm{d}\lambda}, \tag{2}$$

$$Z = \frac{\int_\lambda I_{\mathrm{D65}}(\lambda)\, T(\lambda)\, \bar{z}(\lambda)\, \mathrm{d}\lambda}{\int_\lambda I_{\mathrm{D65}}(\lambda)\, \bar{y}(\lambda)\, \mathrm{d}\lambda}, \tag{3}$$

where $I_{\mathrm{D65}}(\lambda)$ is the spectral power distribution of the D65 illumination standard; $T(\lambda)$ is the simulated reflectance spectrum obtained by FDTD simulation; $\bar{x}(\lambda)$, $\bar{y}(\lambda)$, and $\bar{z}(\lambda)$ are the standard observer functions defined by the Commission Internationale de L'Eclairage (CIE). Then, the chromaticity coordinates can be calculated from the tristimulus values as[35]

$$x = \frac{X}{X+Y+Z}, \tag{4}$$

$$y = \frac{Y}{X+Y+Z}. \tag{5}$$

Since the *RGB* color space is easier to verify the accuracy of the forward and inverse neural networks compared to the CIE 1931-*XYZ* color space. The CIE 1931-*XYZ* color space is converted to *RGB* color space and the results are normalized. The linear relationship between *XYZ* and *RGB* can be described by the following equation[36]

$$\begin{pmatrix} R \\ G \\ B \end{pmatrix} = \begin{pmatrix} 3.2406, -1.5372, -0.4986 \\ -0.9689, 1.8758, 0.0415 \\ 0.0557, -0.2040, 1.0570 \end{pmatrix} \begin{pmatrix} X \\ Y \\ Z \end{pmatrix}. \tag{6}$$

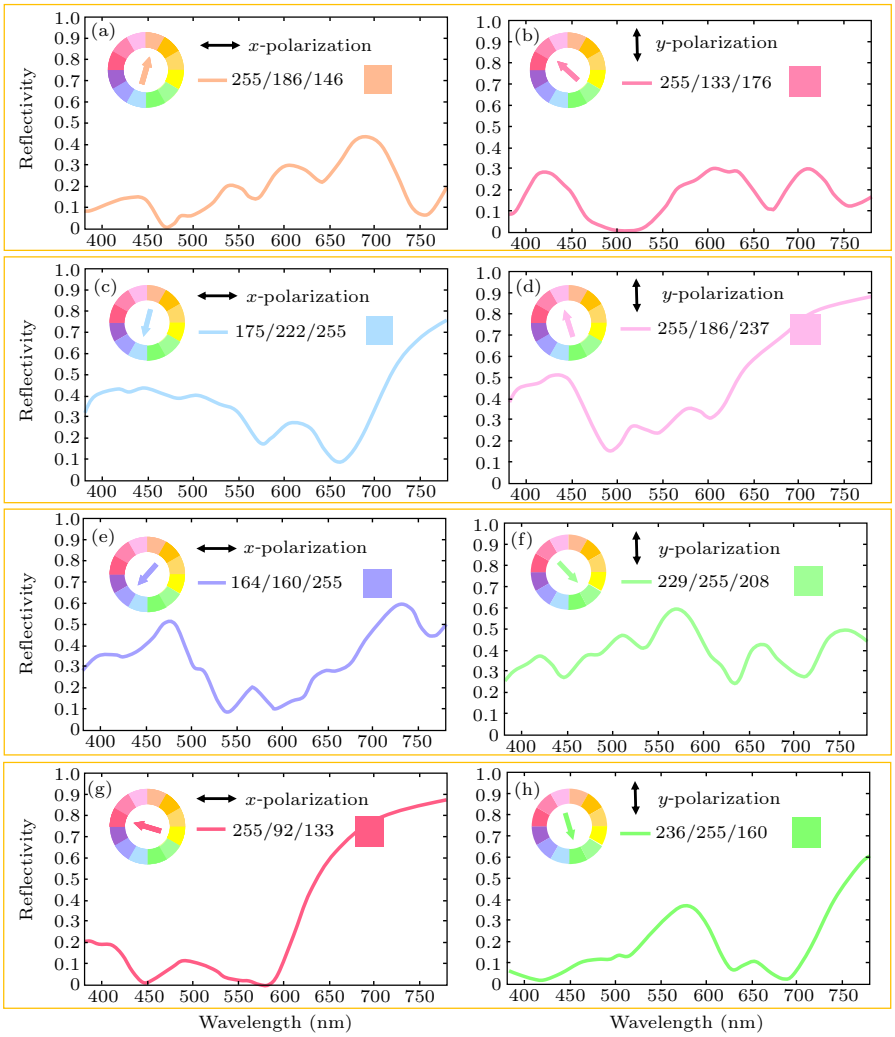


Fig. 2. Multiple sets of polarization-selective coding metasurfaces with the same coding structures presenting reflectance spectra and reflectance colors in the x and y polarization directions. The reflection spectra and colors of (a) structure 1, (c) structure 2, (e) structure 3, and (g) structure 4 in the x-polarization direction. The reflection spectra and colors of (b) structure 1, (d) structure 2, (f) structure 3, and (h) structure 4 in the y-polarization direction.

Selecting 12000 sets of spectral data from the training network, the coordinates (x, y) are calculated and then all of them are plotted in the CIE 1931-XYZ chromaticity diagram, as shown in Figs. 1(b) and 1(c). As shown in the figures, by random coding, this coding metasurface structural color can cover the vast majority of the standard color space in both x and y polarization directions.

While having a relatively wide color coverage, the structural color also has good polarization dependence. When light incidents with two different polarization directions (x and y), the coding metasurface structure can exhibit different colors in the two polarization directions, as shown in Fig. 2. Figures 2(a)–2(h) shows the reflectance spectra and colors of several randomly selected sets of identical coding metasurfaces in both x and y polarization directions.

2.2. Forward prediction network

The basic architecture of the forward LSTM network is built using TensorFlow and Keras. The optimal forward LSTM network contains six hidden layers, as shown in Fig. 3(a). Each intermediate layer of this network uses LeakyReLU (with an alpha value of 0.1) as an activation function, and the output layer uses a sigmoid activation function to compress the output to between 0 and 1. The mean square error (MSE) is chosen as the loss function and the Adam optimizer is selected, setting the learning rate to 0.0001. The input of the forward LSTM network is the 100-bit 0/1 code of the coding metasurface, and the output is the *RGB* value of the structural color with two orthogonal polarization incident lights. During the training process, 10% of the whole 12000 learning datasets are used as the validation datasets, and the other data are used as training data to update the weights on each neuron of the neural network. The batch size is 32. The iteration period of the model parameters is 1500 (epoch = 1500). Moreover, an early stopping procedure is added (patience = 200).

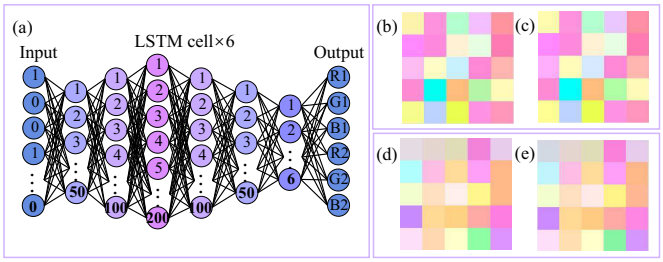


Fig. 3. (a) Schematic diagram of the forward prediction LSTM network for predicting the color values in the two orthogonal polarization directions from the corresponding coding sequences on the coding metasurface. (b) Colors calculated by EM simulation for 25 coding structures in x-polarization direction. (c) Colors predicted by the forward prediction network for 25 coding structures in the x-polarization direction. (d) Colors calculated by EM simulation for 25 coding structures in the y-polarization direction. (e) Colors predicted by forward prediction network for 25 coding structures in the y-polarization direction.

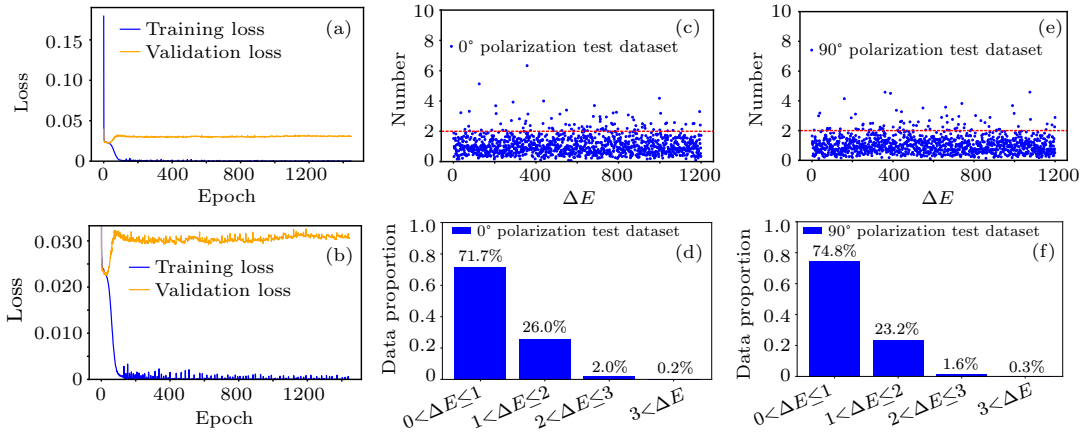


Fig. 4. (a) Training set and validation set loss curves of the forward network. (b) The enlarged loss curves of the training and validation set loss curves of the forward network. (c) The color difference between the predicted color and the true color in the 0° polarization direction ΔE. (d) The distribution statistics of the color difference ΔE between the predicted color and the target color for the 0° polarization direction. (e) The color difference between the predicted color and the true color for the 90° polarization direction ΔE. (f) The distribution statistics of the color difference between the predicted color and the target color in 90° polarization direction ΔE.

The training results show that the magnitude of the normalized mean square error (NMSE) of the model in the training set is 10^{-4}, and the model loss curves can be seen in Figs. 4(a) and 4(b). Figures 3(b)–3(e) show the difference between the colors predicted by the LSTM network and those calculated by the FDTD simulation in the x and y polarization directions. All 25 colors are randomly selected from 1200 test datasets that did not participate in training. As can be seen, the difference between the two methods is so small that it cannot be distinguished by the naked eye. To further illustrate this point, we further calculated the color difference between the output colors and the target colors of the 1200 sets of data that did not participate in the training of the model via the forward network ΔE, with the following formula:[37]

$$\Delta E = \sqrt{\left(L_{\text{pre}} - L_{\text{true}}\right)^2 + \left(a_{\text{pre}} - a_{\text{true}}\right)^2 + \left(b_{\text{pre}} - b_{\text{true}}\right)^2}, \quad (7)$$

where L_{pre}, a_{pre}, and b_{pre} are the predicted values of the forward network; L_{true}, a_{true}, and b_{true} are the target values in the test set. The values and distributions of the color difference ΔE are shown in Figs. 4(c)–4(f). The result shows that the proportion of $\Delta E \leq 2$ in the color difference ΔE between the colors predicted by the model and the target colors in the 0° polarization direction and 90° polarization direction is about 98% on average, and the average color difference $\Delta E = 0.797591$. Generally speaking, when $\Delta E \leq 2$ it is difficult for the human eye to distinguish the difference between colors.[37,38] This indicates that the prediction accuracy of this forward prediction network is about 98%.

2.3. Reverse design network

The inverse LSTM network is the core part of the inverse design. It should be clear that there are cases in the dataset where different coding sequences correspond to the same color. In this case, the correspondence of the data is expressed as many-to-one in the forward network and as one-to-many in the inverse network. This will produce the problem of non-uniqueness of the output value of the inverse network, and lead to the adjustment direction of the inverse network parameter values can not be determined, which makes the model can not converge normally.

In order to solve the problem of the non-uniqueness of the output values of the inverse network and the inability of the model to converge normally, we construct a cascade network with reference to the feedback mechanism of supervised learning. The cascade network takes the inverse network as the generator and the forward network as the discriminator. During the training process, the parameters of the inverse network are set to be trainable, while the parameters of the forward network are locked to achieve the purpose of supervising the training of the inverse network with the forward network.

At this point, after the *RGB* values of the target colors (R1, G1, B1, R2, G2, B2) are input to the inverse network during the training process, the inverse network outputs a coding metasurface structure expressed as a sequence of 0/1. This coding metasurface structure (0/1 sequence) is input to the forward network, and the *RGB* values of the corresponding colors (R1′, G1′, B1′, R2′, G2′, B2′) are computed by the forward network. Meanwhile, the coding metasurface structure (0/1 sequence) is recorded. The mean square error between (R1, G1, B1, R2, G2, B2) and (R1′, G1′, B1′, R2′, G2′, B2′) is computed and recorded.

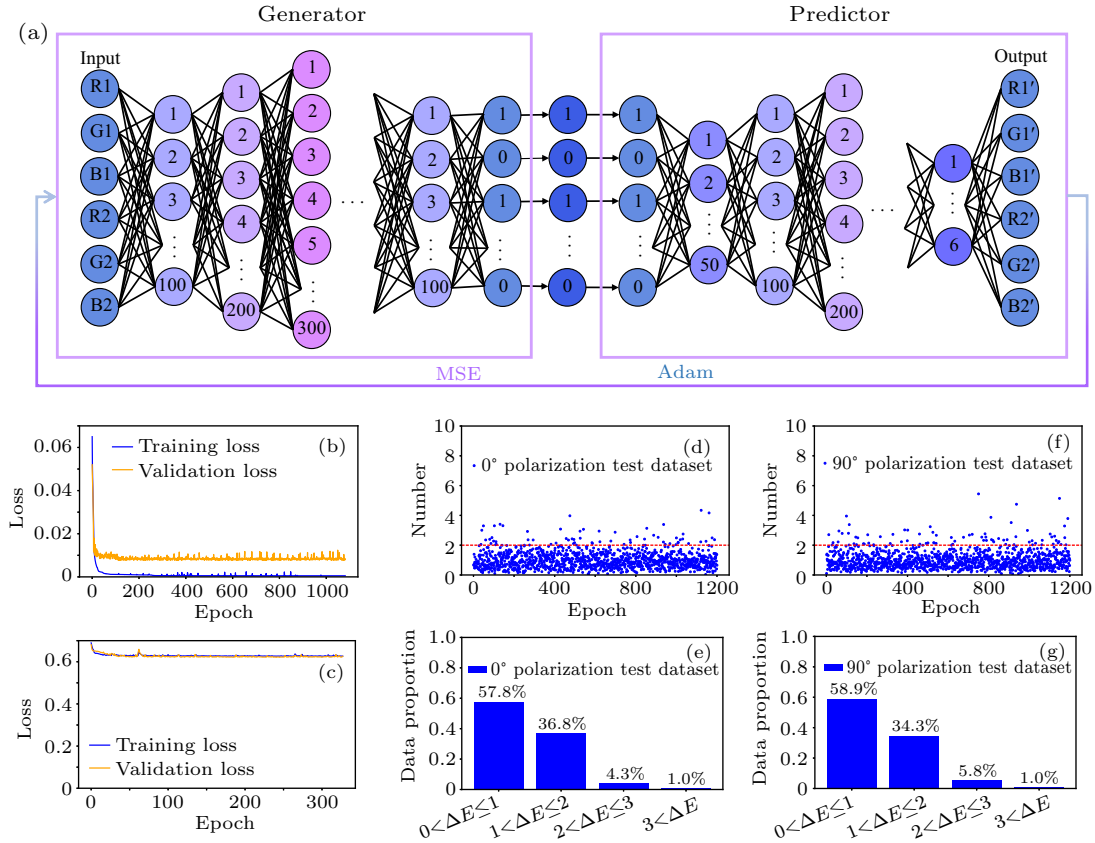


Fig. 5. (a) Schematic diagram of the cascade LSTM network. (b) Training set and validation set loss curves for the cascade network. (c) Training set and validation set loss curves of the directly trained inverse network. (d) The color difference between the predicted color and the true color for the 0° polarization direction ΔE. (e) The distribution statistics of the color difference ΔE between the predicted color and the target color for the 0° polarization direction. (f) The color difference between the predicted color and the true color for the 90° polarization direction ΔE. (g) The distribution statistics of the color difference ΔE between the predicted color and the target color in 90° polarization direction.

Train the network again, a new mean square error will be obtained. If the new mean square error is decreased, the coding metasurface structure (0/1 sequence) record is refreshed with the new one. Then the network will continue to be trained again. If the mean square error is no longer decreasing in many subsequent (patient value times) training sessions, the network will stop training. The latest coding metasurface structure (0/1 sequence) is the designed structure. Through this process, the inverse network can obtain a coding metasurface structure (0/1 sequence) for a target color, thus solving the problem of non-uniqueness of the output values and the inability to converge when directly training the inverse network. This process and the cascade network can be seen in Fig. 5(a).

In this cascade network, the generator contains 8 hidden layers, where each intermediate layer uses LeakyReLU (with an alpha value of 0.1) as an activation function and the output layer uses a sigmoid activation function. The mean square error (MSE) is chosen as the loss function, the Adam optimizer is selected and the learning rate is set to 0.0001. 10% of the whole 12000 training dataset is used as validation dataset and other data are used as training data. The batch size is 32. the model is preset to have an iteration period of 2000 (epoch = 2000). In addition, an early stopping procedure (patience = 100) is added. The results are shown in Fig. 5(b), where the loss value of the model in the training set is of the magnitude of 10^{-3}. As a comparison, the loss curves when the inverse network is trained directly are shown in Fig. 5(c), where the model consistently has large loss values and fails to converge. To further evaluate the generalization performance of the model, we input 1200 sets of data that are not involved in the model training into the model and analyze the color difference of its output colors. As shown in Figs. 5(d)–5(g), the output shows no more than 7% color difference $\Delta E > 2$ in both polarization directions, with an average color difference $\Delta E = 1.003865$. Thus, with reference to the excellent performance of the forward network, the accuracy of the inverse network trained by this cascade structure can be determined to be about 93%."

Figure 6 illustrates the inverse network training method used to coding metasurface polarization-selective structural colors and the validation process of the inverse network design results.

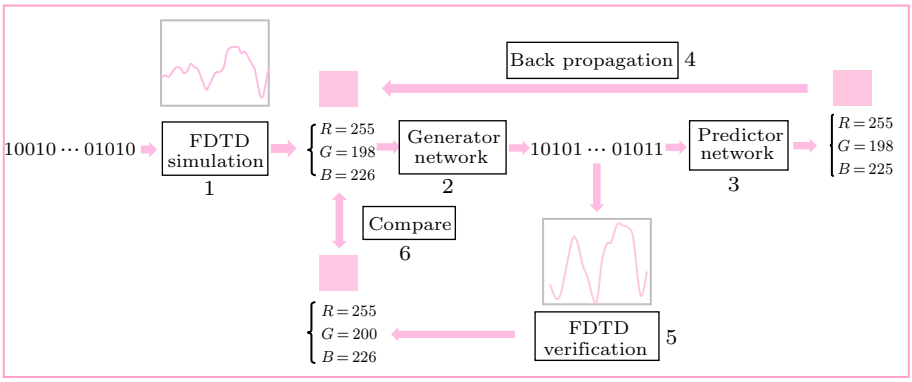


Fig. 6. The inverse network training method used to coding metasurface polarization-selective structural colors and the validation process of the inverse network design results.

The $1 \rightarrow 2 \rightarrow 3 \rightarrow 4$ is the training method of the inverse network. Firstly, the reflection spectrum of a particular coding metasurface under white light irradiation at a particular polarization angle is calculated by the FDTD method, and the calculation result is converted into the *RGB* values of the corresponding colors (the *RGB* values of a particular structure in Fig. 6 are $R = 255$, $G = 198$, and $B = 226$); then, the *RGB* values are inputted into the inverse network to generate a coding sequence of the desired coding metasurface; next, this coding sequence is fed into a parameter-locked high-precision discriminator network to predict the color; finally, the output data of the discriminator network is compared with the input data of the generator by a back-propagation algorithm and the difference between the two data is minimized. The final output *RGB* values are $R = 255$, $G = 198$, $B = 225$, and the error between the two sets of *RGB* values is almost negligible.

The $1 \rightarrow 2 \rightarrow 5 \rightarrow 6$ is the verification process of the result of reverse network design. The operation process and purpose of 1 and 2 are the same as that of training the inverse network. 5 calculates the coding sequence output from the generator network through the FDTD method to obtain the reflected light spectrum and color values ($R = 255$, $G = 200$, $B = 226$); and 6 compares the colors presented by the reverse-designed coding metasurface with the actual target colors. The color difference between the two colors is so small that it is almost impossible to observe the color difference with the naked eye.

It is noteworthy that the coding sequences used for the FDTD simulation are completely different from the coding sequences input from the forward network to the reverse network, but the structure colors they can present are almost the same. This phenomenon proves the existence of the case where different structures in the dataset correspond to the same

color and also proves that the solution proposed in this paper for the problem of non-uniqueness of the model output values and the difficulty of convergence of the model caused by this problem is a practical approach.

Finally, an image with some text information is encrypted by using the inverse prediction network in the paper, as shown in Fig. 7.

In the first place, the *RGB* values of all pixel points on the image are extracted. Then these values are recorded into a dataset as the target color in the *x*-polarization direction. The datasets are set as the inputs of the inverse prediction neural network. Next, the *RGB* values of the dataset in the *y*-polarization direction are randomly taken to other specific values in sRGB as much as possible, to encrypt the specific information contained in the image. Following this, the dataset is input into the inverse network. A coding sequence satisfying the target *RGB* values in both the *x* and *y* directions is obtained. After the inverse network generates corresponding coding sequences based on the target color, these coding sequences are sequentially input to the high-precision forward prediction neural network for prediction.

The target image and the predicted images in the two orthogonal polarization directions are shown in Figs. 7(a)–7(c). The inverse neural network shows excellent performance in coding metasurface structural color design with high accuracy, not only presenting the desired image information completely in a specific polarization direction but also hiding the picture information almost completely in the other polarization direction.

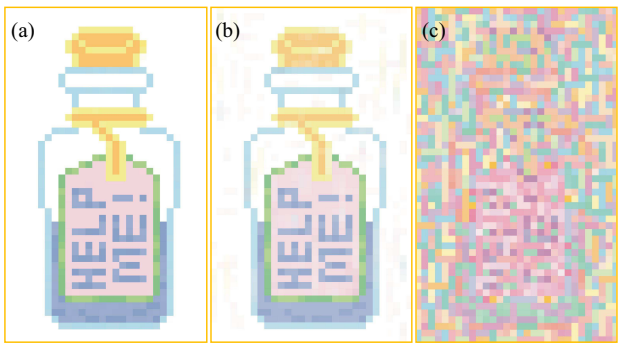


Fig. 7. (a) The target image with specific information. (b) The predicted image is presented in the *x*-polarization direction after the image passes through the cascade network. (c) The predicted image is presented in the *y*-polarization direction after the image passes through the cascade network.

3. Conclusion

In this paper, the inverse design of the polarization-selective coding metasurface structural color has been proposed and studied based on LSTM networks. The result shows that both forward prediction network and inverse prediction network based on LSTM network have good prediction performance and can realize optical encryption of images. In addition, the feedback mechanism of supervised learning is also introduced in the training of the inverse network, and the problem of non-uniqueness and the inability to converge properly, which exists when the inverse network is trained directly, is solved by constructing a cascade network. This work will promote the development of polarization-selective coding metasurface structural color inverse design based on LSTM networks and provide a new idea for practical applications such as optical image encryption and anti-counterfeiting based on polarization-selective coding metasurface structural color.

Acknowledgement

Project supported by the National Natural Science Foundation of China (Grant Nos. 62375137 and 62175114).

References

[1] Yu N F, Genevet P, Kats M A, Aieta F, Tetienne J P, Capasso F and Gaburro Z 2011 *Science* **334** 333
[2] Xie X, Pu M B, Jin J J, Xu M F, Guo Y H, Li X, Gao P, Ma X L and Luo X G 2021 *Phys. Rev. Lett.* **126** 183902
[3] Kumar K, Duan H G, Hegde R S, Koh S C W, Wei J N and Yang J K W 2012 *Nat. Nanotechnol.* **7** 557
[4] Roberts A S, Pors A, Albrektsen O and Bozhevolnyi S I 2014 *Nano Lett.* **14** 783
[5] Wu B Y, Wang M J, Sun Y S, Wu F, Shi Z X and Wu X H 2022 *Adv. Compos. Hybrid Mater.* **5** 2527
[6] Yan Z D, Tang C J, Wu G H, Tang Y M, Gu P, Chen J, Liu Z Q and Huang Z 2021 *Nanomaterials* **11** 63
[7] Pei Y, Sang T, Mi Q, Wang J C and Wang Y K 2022 *J. Opt.* **24** 024001
[8] Reza M R 2021 *Photon. Nanostruct.* **43** 100883
[9] Wang X Y, Chen M, Zhao W L, Li R J, Shi X Y, Han W H, Liu J B, Teng C X, Deng S J, Cheng Y and Yuan L B 2024 *Opt. Laser Technol.* **170** 110190
[10] Liu Y Q, Chen W Q, Du X M, Shu Y C, Wu L J, Ren Z R, Yin H C, Sun J H, Qi K A, Che Y X and Li L S 2023 *Result Phys.* **47** 106366
[11] Cui T J, Qi M Q, Wan X, Zhao J and Cheng Q 2014 *Light Sci. Appl.* **3** e218
[12] Wei Y X, Zhao M and Yang Z Y 2022 *Opt. Lett.* **47** 5344
[13] Wu Z P, Zhang Z Q, Xu Y J, Zhai Y S, Zhang C R, Wang B Z and Wang Q L 2022 *Opt. Lett.* **47** 4548
[14] Li H X, Long B, Wang T, Zhou F, Xu Y L and Zhang Z P 2024 *Opt. Commun.* **554** 130205
[15] Cheng T, Ma Y K, Zhao H H, Fei T H, Liu L H and Yang J Y 2023 *Nanophotonics* **12** 3121
[16] Zhou Y T, Wang Q Y, Ji Z Q and Zeng P 2022 *Photonics* **9** 402
[17] Wen Y, Lin J, Chen K L, Lin Y S and Yang B R 2022 *Opt. Laser Technol.* **150** 108004
[18] Gu J T, Liu Y, Meng N N, Sahmuganathan V, Tan S C, Sudijono, J, Tang J C, Venkatasubramanian E, Mallick A, Tjiptoharson F, Rezaei S D, Teo S L, Zhu Q, Chen Y J, Lin M, Dong Z G and Loh K P 2023 *Adv. Opt. Mater.* **11** 2202826
[19] Wang L, Wang T, Yan R Q, Yue X Z, Wang H M, Wang Y D, Zhang J Y, Yuan X Y, Zeng J W and Wang J 2023 *Nano Lett.* **23** 5581
[20] Li D Y, Wang W, Chu L Y and Deng N N 2023 *Nano Lett.* **23** 9657
[21] Yang B, Liu W W, Li Z C, Cheng H, Choi D Y, Chen S Q and Tian J G 2019 *Nano Lett.* **19** 4221
[22] Namhwa K and Seok E H 2023 *J. Korean Phys. Soc.* **82** 166
[23] Liu X, Huang Z and Zang J F 2020 *Nano Lett.* **20** 8739
[24] Zhang R, Guo X, Qiu H, Liu X, Han M, Jia T and Cheng H 2021 *JETP Lett.* **114** 371
[25] Li X Z, Shu J, Gu W H and Gao L 2019 *Opt. Mater. Express* **9** 3857
[26] Liu Z C, Zhu D Y, Rodrigues S P, Lee K T and Cai W S 2018 *Nano Lett.* **18** 6570
[27] Liu Z C, Zhu D Y, Lee K T, Kim A S, Raju L and Cai W S 2020 *Adv. Mater.* **32** 1904790

[28] Zhu L, Zhang C, Dong L, Rong M X, Gong J Y and Meng F Y 2023 *Phys. Scr.* **98** 105501
[29] Ding Z P, Su W, Luo Y L, Ye L P, Li W L, Zhou Y H, Zou J F, Tang B and Yao H B 2024 *Nanoscale* **16** 1384
[30] Ghorbani F, Shabanpour J, Beyraghi S, Soleimani H, Oraizi H and Soleimani M 2021 *Appl. Phys. A* **127** 869
[31] Sajedian I, Kim J and Rho J 2019 *Microsyst. Nanoeng.* **5** 27
[32] Wang J H, Lin Z C, Fan Y, Mei L Y, Deng W Q, Lv J W and Xu Z J 2022 *Materials* **15** 7008
[33] Ma T G, Wang H Z and Guo L J 2024 *Opto-Electron. Adv.* **7** 240062
[34] Palik E D 1985 *Handbook of Optical Constants* (Academic Press)
[35] Duan X Y, Kamin S and Liu N 2018 *Nat. Commun.* **8** 14606
[36] Xu Y L, Li H X, Zhang X, Liu W J, Zhang Z P, Qin S J and Liu J T 2021 *Opt. Express* **29** 32491
[37] M. Quinten 2001 *Appl. Phys. B* **73** 317
[38] Costa T L, Hamer R D, Nagy B V, Barboni M T S, Gualtieri M, Boggio P S and Ventura D F 2015 *Exp. Brain Res.* **233** 1213